Improved Location of Microseismic Events in Borehole Monitoring by Inclusion of Particle Motion Analysis: a Case Study at a CBM Field in Indonesia

Rexha Verdhora Ry[1], T. Septyana[1,3], S. Widiyantoro[2], A. D. Nugraha[2], A. Ardjuna[4]

[1]Graduate Program of Geophysical Engineering, Faculty of Mining and Petroleum Engineering, Institut Teknologi Bandung, Ganesha 10, Bandung 40132, Indonesia
[2]Global Geophysics Research Group, Faculty of Mining and Petroleum Engineering, Institut Teknologi Bandung, Ganesha 10, Bandung 40132, Indonesia
[3]BP Indonesia
[4]SKK Migas Indonesia

E-mail: rexha.vry@gmail.com

Abstract. Microseismic monitoring and constraining its hypocenters in and around hydrocarbon reservoirs provides insight into induced deformation related to hydraulic fracturing. In this study, we used data from a single vertical array of sensors in a borehole, providing measures of arrival times and polarizations. Microseismic events are located using 1-D velocity models and arrival times of P- and S-waves. However, in the case of all the sensors being deployed in a near-vertical borehole, there is a high ambiguity in the source location. Herein, we applied a procedure using azimuth of P-wave particle motion to constrain and improve the source location. We used a dataset acquired during 1-day of fracture stimulation at a CBM field in Indonesia. We applied five steps of location procedure to investigate microseismic events induced by these hydraulic fracturing activities. First, arrival times for 1584 candidate events were manually picked. Then we refined the arrival times using energy ratio method to obtain high consistency picking. Using these arrival times, we estimated back-azimuth using P-wave polarization analysis. We also added the combination of polarities analysis to remove 180^o ambiguity. In the end, we determined hypocenter locations using grid-search method that guided in the back-azimuth trace area to minimize the misfit function of arrival times. We have successfully removed the ambiguity and produced a good solution for hypocenter locations as indicated statistically by small RMS. Most of the events clusters highlight coherent structures around the treatment well site and revealed faults. The same procedure can be applied to various other cases such as microseismic monitoring in the field of geothermal and shale gas/oil exploration, also CCS (Carbon Capture and Storage) development.

1. Introduction

Microseismic monitoring involves the passive seismic recording of acoustic emissions from certain event source known as microearthquake. Microearthquake is defined as a small magnitude earthquake, and it often is referred to as microseismic events. Microseismic events are associated with naturally occurring of artificially induced fracture movements, resulting in inelastic geomechanical fracture

deformation. Due to it, in the hydraulic fracturing treatment, microseismic monitoring is the powerful technology to image stimulated hydraulic fractures [1].

Typically, the passive recordings are used to detect microseismic events and to constrain its hypocenter location and attribute. Accurate event locations are important to study the induced fractures. Most methods used to determine the location assume a velocity model and minimize the difference between the observed and predicted arrival times of P- and S-wave phases at some receivers, e.g. [2,3,4,5]. Several factors control this location accuracy; one of them is source-receiver geometry [6]. Geophone array deployed in a single near-vertical borehole has often been used for microseismic monitoring of hydrocarbon reservoir and hydraulic fracturing. This geometry may lead to ambiguous solution due to the ambiguity of misfit function in the horizontal direction. The use of a 1D velocity model and a near-vertical array of sensors also leads to an 180^o ambiguity where the event can be either side of the monitoring well. In contrast, these ambiguities do not occur in monitoring as the stations are located on the surface.

In this paper, we apply a location procedure using the inclusion of P-wave particle motion to constrain the initial source location. The information of P-wave polarization is required to constrain the direction of the source location from receiver [7,8]. We also added the combination of polarities analysis to remove 180^o ambiguity. Then, we determined the hypocenters location using guided-grid-search method. This procedure was applied to a dataset acquired during fracture stimulation of particular coalbed methane (CBM) field in Indonesia.

2. Event Location Workflow

The data processing for locating microseismic events consists of 4 steps: 1) manually picking of the P- and S-wave arrival times, 2) hodogram analysis of P-wave polarization to estimate back-azimuth, 3) removal of 180^o ambiguity using the combination of polarity analysis, 4) inversion process using guided grid search method.

2.1. Arrival time picking

One of the major contributors to errors in event location is an error in arrival time phase picking [6]. An automated procedure can be applied in this picking by comparing a short-term average and a long-term average of the signal [9]. This automated procedure can help to overcome the problems of consistency and time-consuming. However, a disadvantage of the automated procedures is that they lack consistency in where the pick is placed with respect to the waveform [7].

In this paper, we picked the phase of P- and S-wave manually, although it is very time-consuming. We insist that manually picking is the better way to reduce error in event location, as long we perform the refinement of arrival time picking. We refined the arrival times using modified energy ratio (MER) method to reduce a human error while picking and obtain high consistency picking. The MER algorithm is an extension of STA/LTA in which the pre- and post-sample windows are of equal size. The energy ratio (ER) at the *i*-th time sample is given by [10],

$$MER(i) = \left(\frac{\sum_{j=i}^{i+w} x_j^2}{\sum_{j=i-w}^{i} x_j^2} |x_i|\right)^3 \quad (1)$$

where *w* is the window length and *x* is the input series. Because the energy ratio function is computed using post- and pre-sample windows, the time index associated with the maximum of the MER represents the arrival time pick.

2.2. P-wave polarization

We need to estimate P-wave polarization to constrain the direction of source location from a receiver. Since the P-waves are vertically and radially polarized, the vector of P-wave amplitude can be used to calculate the back-azimuth to the source. We performed a hodogram analysis of P-wave polarization

by cross plotting the signal amplitude on the horizontal components, e.g. [8,11]. This hodogram depicts a graphical movement of the ground motion (eg., fig. 1b).

First, we cut the very first signal of P-wave after it arrived to obtain a sharp P-wave linear polarization (shown in fig. 1a). We applied principal component analysis on the relative signal amplitude to calculate a principal direction of horizontal components: A_N for the North-South component and A_E for the East-West component. We then calculate the signal polarization azimuth $\emptyset$ [12] by

$$\emptyset = tan^{-1}\frac{A_E}{A_N}. \quad (2)$$

2.3. *Combination of Polarity Analysis*

There is an ambiguity of 180° where the event can be either side of the monitoring well. It occurs due to the limitation of the solution from arctangent. Therefore, the solution will be limited by

$$-90 \leq \emptyset \leq 90. \quad (3)$$

Therefore, we should add 180° to the azimuth we obtained based on the combination of polarities. The first polarity can be up (positive) or down (negative) so it can be used to get the correct back-azimuth. If the first motion on the vertical component of the P is upward, then the radial component of P is directed away from the source. The opposite is true if the P-polarity is negative [12]. This combination is shown in Table 1.

As an example in fig. 1, we could determine the first polarity for every component. The first polarity for vertical, N-S, and E-W respectively is positive, positive, and negative. The back-azimuth calculated from P-wave polarization is -50° or 310°. However, based on the combination of polarities, we must add 180° to our solution. So, the back-azimuth of source location from the receiver is 130°.

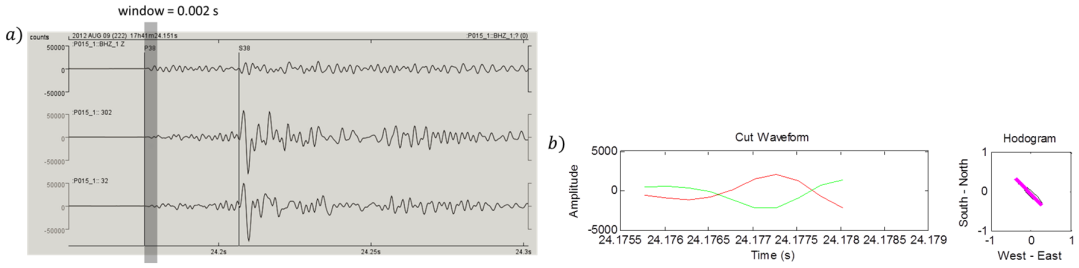

Figure 1. An example of P-wave polarization analysis: a) the recorded signal waveform and very first part of P-wave windowing; b) the cut waveform and the hodogram for horizontal component (the black line shows the cross plotting and the magenta line shows principal direction).

Table 1. Combination of polarities and cases where 180° has to be added to the calculation

Z	+	–	+	–	+	–	+	–
N	+	+	–	–	–	–	+	+
E	+	+	+	+	–	–	–	–
Add	180	0	0	180	0	180	180	0

2.4. *Event location*

The last step of our procedure is the inversion process to obtain the location of the microseismic event. We used guided grid search to produce accurate hypocenter location. Grid search method work to minimize an objective function by searching trough all points systematically in the model space we set [13]. The objective function used is the misfit function, the difference between the observed and calculated arrival times of P- and S-wave phases at a number of receivers.

Since the origin time of the microseismic event is an unknown parameter, we used another way of incorporating differential arrival times and their associated calculated travel times into the hypocenter determination problem. We used master station method [13,14] which is minimizing all combinations of arrival times and sensors. The objective function for the minimization of all combinations of arrival times and sensors is given by

$$E(i) = \sum_{j=1}^{N-1} \sum_{k=1+1}^{N} \left[\left(t_j^{obs} - t_k^{obs} \right) - \left(T_{ij}^{cal} - T_{ik}^{cal} \right) \right]^2 \quad (4)$$

which is the generalization of minimizing the misfit. In equation (4), t_j^{obs} is the observed arrival times at receiver *j*; t_k^{obs} is the observed arrival times at receiver *k*; T_{ij}^{cal} is the calculated travel time from source *i* to receiver *j*; and T_{ik}^{cal} is the calculated travel time from source *i* to receiver *k*.

From step 2 and 3, we already had the back-azimuth of source location from a receiver. Using this back-azimuth, we could constrain the model space in our grid search inversion process. We can also set a tolerate angle towards the back-azimuth. We set the model space to search systematically in that direction (shown in fig 3). So, we can reduce the ambiguity of misfit distribution using this technique.

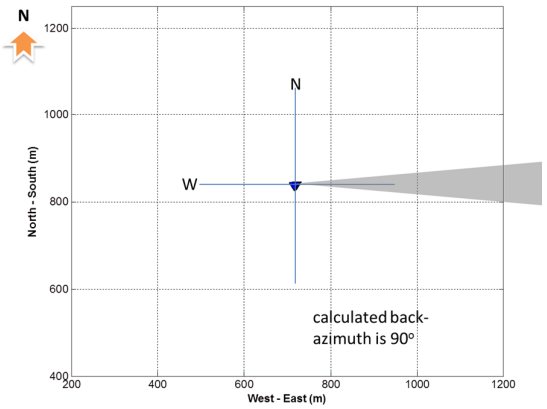

Figure 2. The schematic diagram showing the grid search area from a receiver (gray zone), which is constrained by back-azimuth and 5° tolerate angle.

3. Application to The CBM Field

Hydraulic fracture treatment was conducted in particular coalbed methane (CBM) field in Indonesia. The production stage in this field is still on development stage. Therefore, the purpose of this treatment is to develop and to increase the permeability of the reservoir. The fracture stimulations were divided into 11-days of injection stages, located in the treatment well (Fig. 3a). In this paper, the procedure was applied to a dataset acquired during 1-day monitoring which had the most seismicity. The 1D velocity model was derived from sonic logs recorded in the treatment well. The logs were smoothed to interface blocked model (Fig. 3). Every single block represents a lithological group in this area study. The thin layered block with low velocity represents coal-bed where the methane gas lied.

The microseismicity was recorded using eight downhole seismometers with sampling rates of 4000Hz or 0.25 milliseconds (Fig. 3a-b). The earlier step is the event identification. We identified the event based on STA/LTA analysis [9]. During the 1-day monitoring, we had identified up to 1700 microseismic events. This number of events is considered as a high seismicity if compared with the other days. Then, the first step of the procedure is the manual picking of P- and S-wave arrival times. However, not all identified events had a good signal to noise ratio. We only selected the events with the high confidence of arrival times picking. So, the number of microseismic events is reduced to 1584 events.

The next step is the estimation of back-azimuth using P-wave polarization. Using the hodogram analysis, we calculated the polarization direction in every station for certain event. Fig 4 shows an example of the polarization that recorded in every station. The refinement of arrival times picking is helpful to obtain the good consistency of polarization direction in every station. The back-azimuth for this certain event is defined as the average value of these polarization directions that have been corrected using the combination of polarities.

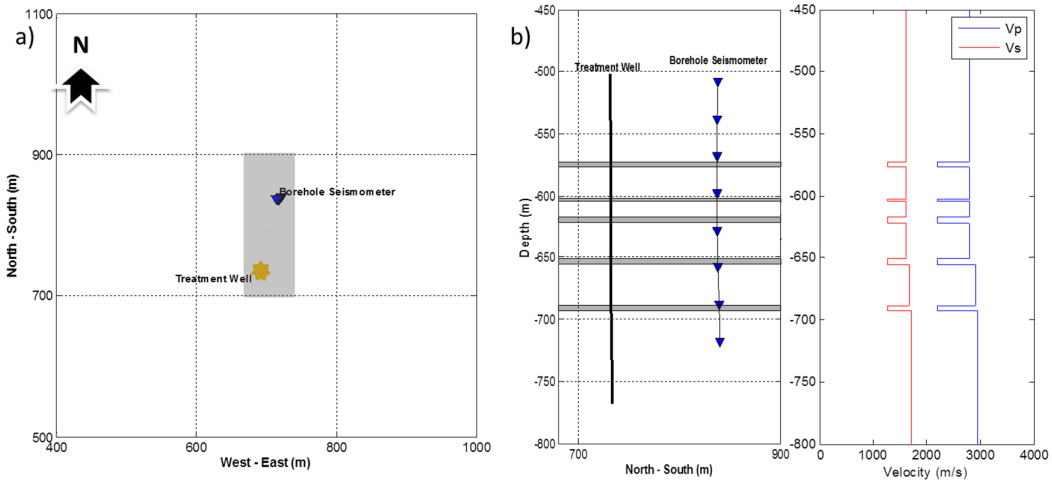

Figure 3. (a) Map view of borehole geometry at the study area. (b) The geometry of downhole seismometer and the one-dimensional velocity model for P- and S-wave which used in this study.

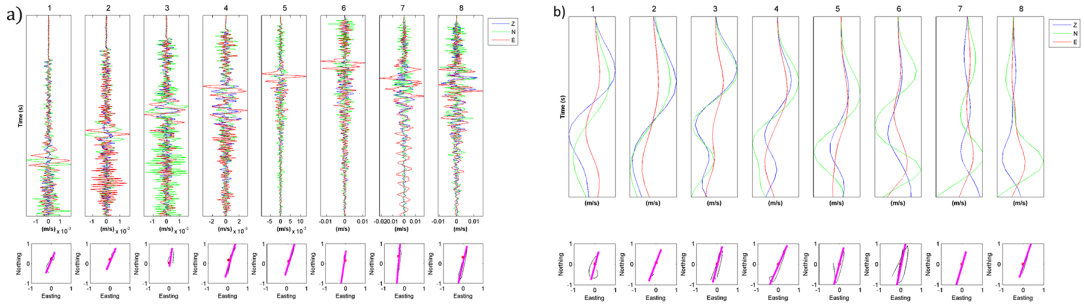

Figure 4. An example of recording waveform and hodogram analysis for every station, in a display of (a) the long waveform and (b) the cut waveform according to the window.

4. Result and Discussion

The totals of 1584 events were successfully located using guided grid search (Fig. 5). The microseismic events occurred at a depth between 570 to 580 meters. It is well correlated with the hydraulic fracturing location. The injection during that day located in the first layer of coal-bed (depth of 572 meters), so the distribution in depth comparison is reasonable.

Since the sensor geometry used is single vertical borehole array, the possibility of miss interpretation exists in a horizontal plane. From the microseismic event distribution in a horizontal plane, we can divide them into 2 clusters: (1) South cluster, where the events distributed in SE-NW direction started from treatment well; (3) East cluster, where the events distributed in SE-NW direction like the first cluster, but they have a gap from treatment well.

The South cluster is the most reasonable cluster in this result. The previous study inferred that there is a fault with a Southeast-Northwest direction around the treatment well. In this cluster, fractures were generated around treatment well. As more fluid was injected, the fractures continue to widen and grow outward from the well. Most of the fractures generated during hydraulic fracturing could have followed the same preexisting fractures, opening them, causing a slip on them, and getting filled with some proppant, e.g. [16].

The East cluster, nevertheless, is the most interesting distribution. The microseismic events occurred in the Southeast-Northwest direction like the South cluster but located not along that. There is a gap in the middle that separated this cluster. The possibility is that triggered seismic events occurred in this area. The triggered seismicity can occur if a fault is close to failure and requires comparatively less pressure change to cause an earthquake [1]. Other study inferred that there is an ancient fault in this area. However, due to the lack of the data, it is not confirmed yet. Furthermore, we need to confirm them by their source characterization like magnitude and focal mechanism.

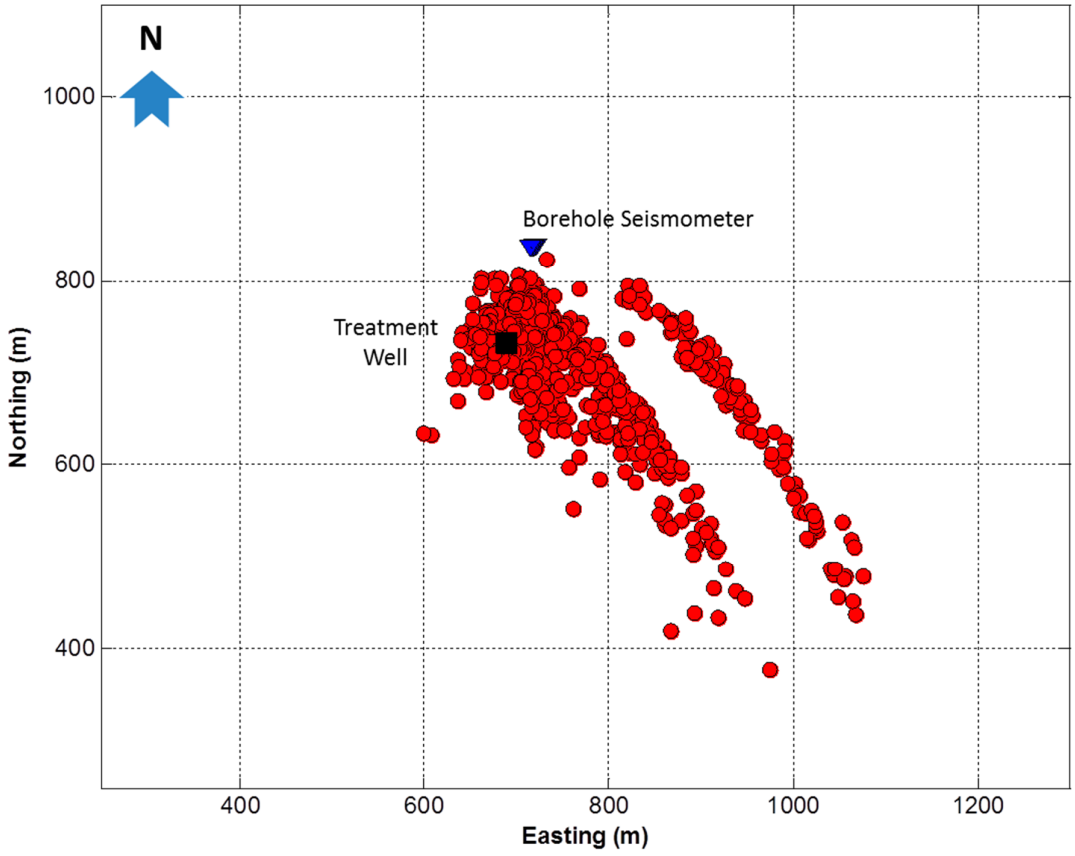

Figure 5. Map view of microseismic event locations (red dot) at certain coalbed methane (CBM) Field in Indonesia, stimulated by hydraulic fracturing treatment during 1-day monitoring. The black square is the treatment well, and the blue reverse triangle is monitoring well.

5. Conclusions

We have applied a procedure to improve the microseismic event location and remove 180^{o} ambiguity inflicted by using a single vertical borehole array. We found that the event distribution in East cluster is unusual but yet still questionable. The next step of our research is to confirm this cluster by analyzing its source characterization like magnitude and focal mechanism.

The distribution of microseismic events is very reliable in both depth and horizontal plane for the South cluster. This events cluster highlights coherent structures around treatment wells and inferred faults. However, the reliability of this procedure will depend on the quality of arrival times picking. The same procedure can be applied to various other cases such as microseismic monitoring in the field of CCS (Carbon Capture and Storage), geothermal, and shale gas/oil exploration development.

Acknowledgement
The authors greatly acknowledge SKK Migas Indonesia for providing data in this study; Laboratory of Near Surface Geophysics, Faculty of Mining and Petroleum Engineering, Institut Teknologi Bandung (FTTM ITB) and Indonesia Endowment Fund for Education (LPDP) for supporting this study.

References
[1] Maxwell S 2014 Microseismic imaging of hydraulic fracturing: Improved engineering of un-conventional shale reservoirs *Publication of SEG*.
[2] Foulger G R 1982 *Geothermics* **11** 259-268
[3] Nishi K 2005 Hypocenter Calculation Software GAD (Geiger's Method with Adaptive Damping) ver 1. *JICA report*
[4] Ry R V and Nugraha A D 2015 Improve earthquake hypocenter using adaptive simulated annealing inversion in regional tectonic, volcano tectonic, and geothermal observation *AIP Conference Proceedings* **1658** 030004
[5] Ry R V, Priyono A, Nugraha A D, and Basuki A 2015 Seismicity study of volcano-tectonic in and around Tangkuban Parahu active volcano in West Java region, Indonesia *AIP Conference Proceedings* **1730** 020004
[6] Pavlis G L 1986 *Bull. of the Seismological Society of America* **76**(6) 1699–1717
[7] Jones G A, Raymer D G, Chambers K, and Kendall J M 2010 *Geophysical Prospecting* **58** 727–737
[8] Moriya H 2008 *Geophysical Prospecting* **56** 667–676
[9] Earle P S and Shearer P M 1994 *Bull. of the Seismological Society of America* **84**, 366–376.
[10] Akram J and Eaton D W 2016 *Geophysics* **81** 67-87
[11] Alessandrini B, Cattaneo M, Demartin M, Gasperini M, and Lanza V 1994 *Annali di Geofisica* **37**
[12] Havskov J and Ottemöller L 2010 Routine data processing in earthquake seismology *Springer*
[13] Jones G A, Kendall J M, Bastow I D, and Raymer D, 2013 *Geophysical Prospecting* **62** 34–49
[14] Zhou H W 1994 *Journal of Geophysical Research* **99**(B8) 15439–15455
[15] Moriya H 2008 *Geophysical Prospecting* **56** 667–676
[16] Rodriguez-Pradilla G 2015 *Leading Edge* **34**(8) 896-902